1   **Revision 2**

2

3   **Oxidation in CSPV experiments involving H$_2$O-bearing mafic magmas: Quantification and**

4   **mitigation**

5

6   **Thomas Shea[1] and Julia E. Hammer[1]**

7   [1] Department of Geology and Geophysics, SOEST, University of Hawaii, 96822,

8   Honolulu, HI, USA.

9

10   **Abstract**

11   A difficulty in performing high temperature (>900°C) experiments on near-liquidus

12   hydrous mafic melts in gas-medium cold-seal pressure vessels (CSPV) is the tendency for H$_2$O

13   in the fluid phase to dissociate and H$_2$ to diffuse through capsule material, leading to progressive

14   oxidation of sample material. Negative consequences include premature stabilization of Fe-Ti

15   oxide phases and commensurate deviation of the liquid line of descent toward silica enrichment.

16   Moreover, time-variance of an intensive variable equal in importance to temperature or total

17   pressure is an unwanted feature of any experimental study. Methodologies commonly employed

18   to mitigate the oxidation problem, not without their own drawbacks, include incorporating CH$_4$

19   into the pressurizing gas, limiting run duration to 24 hours, enclosing samples in Au-alloy

20   capsules, and incorporating solid buffering assemblages to serve as indicators of fO$_2$ excursion.

21   Using the Co-Pd-O system as an fO$_2$ sensor, we investigated progressive oxidation of basaltic

22   andesite at 1010 °C and P$_{H2O}$=150 MPa. Our time-series of 12, 24, 36, 48, and 60 h run durations

23   reveals that oxidation occurs at a very high rate (~3-4 log unit change in fO$_2$ in 48h). Both the

24   variability of $f\text{O}_2$ and magnitude of dehydration-oxidation are considered unacceptable for phase

25   equilibria work. Incorporation of additional CH_4 serves only to offset the progressive oxidation

26   trend toward a lower absolute range in $f\text{O}_2$. Ultimately, rapid oxidation in CSPV hinders the

27   chemical equilibration of experimental charges. Incorporation of a substantial mass of Ni metal

28   powder as an O_2 getter to the outer capsule successfully (a) slows down oxidation (b) stabilizes

29   $f\text{O}_2$ at the Nickel-Nickel Oxide (NNO) buffer after ~20h, (c) allows equilibrium compositions to

30   be attained. Runs much longer than 48h may require one or more steps involving quenching and

31   re-filling the pressure system with CH_4.

32

33   **Keywords:** experimental petrology**,** oxygen fugacity, rates of oxidation, crystallization, chemical

34   equilibrium

35

36

37   **Introduction**

38

39   Experimental petrology explores the effects of environmental conditions (e.g.,

40   temperature T, pressure P, time t, oxygen fugacity $f\text{O}_2$, volatile content X_{fluid}, chemical

41   composition X_{melt}) on the chemical behavior of magmas (e.g., Holloway and Wood 1988).

42   Particularly pertinent to the field of volcanology are experiments that investigate the melting,

43   crystallization, mixing, or vesiculation of magmas and the transport of chemical constituents

44   (e.g., Kouchi and Sunagawa 1983; Blundy and Cashman 2008; Hammer 2008; Zhang and

45   Cherniak 2010). Experiments using magmas of intermediate-to-felsic compositions at crustal

46   pressures (P > 1 atm) and moderate temperatures (T < 900ºC) have increased in frequency in the

2

47   past few decades (e.g., Hammer 2008 and references therein). Similar studies involving hotter (T

48   > 900-950ºC) hydrous mafic magmas at high pressures are sparse (e.g., Sisson and Grove 1993),

49   mostly due to the technical challenges associated with volatile-rich melts at these temperatures.

50   In many instances, high-T experiments involving mafic compositions are run using internally-

51   heated pressure vessels (IHPV; Holloway, 1971; Muncill and Lasaga 1988; Moore et al. 1995;

52   Moore and Carmichael 1998, Pichavant et al. 2002; Berndt et al. 2005; Di Carlo et al. 2006;

53   Simakin et al. 2009), because they allow for large volumes of material and accommodate higher

54   P and T conditions than cold-seal pressure vessels (CSPV; Holloway 1971). Despite their being

55   used more often for colder, more silicic experiments (e.g., Hammer 2008 and references therein),

56   CSPVs are increasingly used for hotter, hydrous experiments (e.g., Metrich and Rutherford 1998;

57   Coombs et al. 2000; Hammer et al. 2002). IHPVs are relatively expensive, difficult to maintain

58   and operate in comparison with CSPV apparatus (Lofgren 1987). Given the growing interest in

59   explosive mafic volcanism (e.g., Houghton and Gonnerman 2008, Di Traglia et al. 2009), there is

60   an opportunity for intensified use of CSPVs in laboratory experimentation involving hydrous

61   mafic magmas. Thus, it is important to evaluate the practical limits of methods already in

62   common use to impose and maintain desired thermodynamic conditions.

63   Oxygen fugacity (fO_2), along with P and T, is widely recognized as an important factor

64   controlling magmatic crystallization sequences and liquid lines of descent (e.g., Muan 1958;

65   Osborn 1959; Sisson and Grove 1993; Toplis and Carroll 1995; Berndt et al. 2005; Hammer

66   2006; Feig et al. 2010). Oxygen fugacity exerts a direct control on the valence state of metal

67   elements (dominantly Fe^{2+}/Fe^{3+} in natural magmas), which, in addition to controlling the

68   appearance of iron-bearing oxides (Carmichael and Nicholls 1967; Toplis and Carroll 1995),

69   dictates how Fe partitions into iron-rich mafic phases such as olivine, pyroxene and amphibole

3

70   (Carmichael and Ghiorso 1990; Carmichael 1991; McCanta et al. 2004). Hence, fO_2 not only

71   affects the presence of certain phases, but their composition (e.g., Mysen 2006) and formation

72   temperatures as well. Because fO_2 can vary by 8-9 orders of magnitude in natural magmas

73   (Carmichael and Ghiorso 1990), it is crucial for experimental apparatus to impose fugacity

74   conditions that are appropriate for a particular natural setting.

75   In 1-atm, high-T experiments, fO_2 is regulated using variable proportions of gas mixtures

76   (e.g., H_2 and CO_2) that react to produce small amounts of free oxygen (Nafziger et al. 1971;

77   Huebner 1987). This setup allows precise control over ambient fO_2 and facilitates examination

78   of the behavior of volatile-poor magmas at planetary surface conditions. In stark contrast,

79   controlling fugacity conditions in high-pressure hydrous experiments to study magmatic

80   processes within the crust is more challenging due to the tendency of dissolved H_2O to

81   dissociate; Hydrogen diffuses through capsule walls, causing the partial pressure of oxygen to

82   progressively increase during the course of the experiment.

83   Relatively low-T (i.e., <900-950 ºC) hydrous experiments are typically carried out in

84   vessels made of Co- or Ni-rich alloys (e.g., 'Stellite-25[®]', 'Waspaloy[®]') that use a supercritical

85   fluid (H_2O) as a pressurizing medium (Edgar 1973). These alloys intrinsically impose fO_2 on

86   enclosed samples that is close to the Co-CoO or Ni-NiO oxygen buffers (Gardner et al. 1995). In

87   contrast, higher temperature (>900-950 ºC) runs entail the use of stronger materials (e.g.,

88   molybdenum-based alloys with Ti and Zr; TZM). In such experimental setups, controlling and

89   monitoring fO_2 is problematic because the pressurizing medium is not H_2O. The lack of such a

90   hydrogen buffer can thus lead to strong H_2 gradients across the experimental capsule wall

91   (Scaillet et al. 1992).

4

92   After a brief summary of available methods to control and monitor oxygen fugacity

93   conditions, we test the degree to which fO_2 varies throughout experiments at high temperatures

94   (>950ºC) and pressures (>100 MPa) involving mafic (basaltic-andesite) magma. We examine the

95   time-variance of fO_2 and thereby the rates of oxidation in CSPV experimental setups. We find

96   that oxidation progresses very rapidly, and prevents the samples from reaching chemical

97   equilibrium. We provide detailed guidelines for preventing rapid increases in fO_2 that involve

98   introducing CH_4 into the pressurizing gas and employing a simplified solid-medium oxygen

99   buffering technique. It is hoped that these provisions will benefit laboratory investigations

100   involving hydrous mafic magmas.

101

102   **Background**

103

104   Controlling fO_2 at high P and T

105

106   Several approaches have been developed to impose a desired fO_2 in experimental runs in

107   high-P studies (c.f. Table 1 for methods adopted in hydrous mafic magma studies using CSPV).

108   The first and simplest procedure involves the introduction of a small amount of hydrogen-

109   containing gas (H_2 or CH_4) into the vessel prior to full pressurization with Ar gas. The CH_4

110   dissociates at experimental temperature to make H_2, thus reducing the gradient in hydrogen

111   across the capsule wall (). We demonstrate below that the increased fH_2 outside the sample

112   capsule shifts the sample fO_2 to more reduced conditions beginning shortly after the vessel is

113   inserted into the high-T furnace. While this procedure allows setting the initial fugacity

114   conditions to a given value, H_2 continuously diffuses out of the capsule and vessel, thus driving

5

115   the system to progressively more oxidized conditions (Scaillet et al. 1992). The 'Shaw-

116   membrane' technique is based on the same principle, the major improvement being that a

117   regulated feed of H_2 gas through a permeable membrane maintains nearly constant fH_2 and fO_2

118   fugacity conditions (Shaw 1963). Hewitt (1978) and later Scaillet et al. (1992) and Schmidt et al.

119   (1995) successfully applied this technique in CSPV; briefly, an H_2-permeable membrane made

120   of Pt or AgPd and mechanically supported by an inert filling (e.g., quartz or alumina grains, to

121   avoid rupture during pressurization) is connected to a hydrogen source and transducer system

122   located outside the vessel by a stainless steel capillary. This technique is, however, not as

123   popular since it requires non-negligible physical modifications to the experimental apparatus

124   (e.g., Gunter et al. 1987; Scaillet et al. 1992) and requires the use of larger volumes of an

125   explosive gas. Another approach was devised by Eugster (1957), and involves the use of solid

126   oxygen buffers such as Ni-NiO (NNO), Co-CoO (CCO) or Fayalite-Magnetite-Quartz (FMQ)

127   inside the noble metal sample capsule that react to maintain fO_2 at a constant value until the

128   buffer is exhausted (Huebner 1971). The solid buffers are usually placed inside sealed capsules

129   along with the starting material, and the various reactions are initiated, capturing or releasing O_2,

130   if the ambient oxygen fugacity varies from the fO_2 value of the corresponding buffer. The main

131   drawback of oxygen buffers is that they are consumed rapidly, particularly at high T where

132   hydrogen diffuses out of the experimental capsules more rapidly, and oxidation reactions are

133   faster (e.g., Scaillet et al. 1992). Matthews et al. (2003) take advantage of the instrinsic buffering

134   redox reactions that occur within alloys dominated by one of various metals (Ni, Co, W, Ti, Fe,

135   C) placed outside sample capsules, usually as filler rods. Wilke and Behrens (1999) use a Boron

136   Nitride (BN) jacket that acts to slow down the loss of H through capsule walls. Both of these

6

137   methods have only been tested at temperatures near the solidus of intermediate to mafic magmas

138   (T=750-850°C).

139

140   Monitoring fO2 conditions at high P and T

141

142   Oxygen fugacity can be monitored directly and in real-time using derivatives of the Shaw-

143   membrane technique described above (e.g., Scaillet et al. 1992) or indirectly using fluid or solid

144   sensors. The Ag-AgCl-HCl fluid fH$_2$ sensor technique takes advantage of H diffusion through

145   the enclosing capsules and the ensuing Ag/AgCl ratio variation changing the pH of the solution,

146   which is measured after quenching (Frantz and Eugster 1973). Taylor et al. (1992) noted that

147   several problems such as fluid evaporation and dilution effects strongly influence the calculation

148   of fO$_2$, and that the range of applicability of this technique was uncertain above T=800°C.

149   Taylor et al. (1992) thus recommended the use of solid redox sensors instead. The latter exploit

150   the capacity of metal-metal oxide systems (e.g., CCO, NNO), alloyed with pure metals (e.g., Pd,

151   Pt), to compositionally self-adjust to changes in fO$_2$. In this fashion, fugacity conditions can be

152   retrieved by analyzing the resulting alloy composition and computing ambient fO$_2$ through a

153   series of calibration equations (O'Neill and Pownceby 1993; Pownceby and O'Neill, 1994). The

154   solid sensor method is preferred since it is readily applicable and requires no mechanical

155   modification to the CSPV setup.

156

157   **Experimental methods**

158

7

159   This section describes the experimental setup used for this investigation. Figure 1a

160   illustrates schematically the various elements that enter our CSPV design along with the main

161   reactions that occur during experimental runs.

162

163

164   Starting material

165

166   A natural sample of basaltic-andesite (bulk composition ~55% wt. SiO_2, ~5%

167   Na_2O+K_2O, Table 1) lava from Mascota volcanic field (Mexico), characterized in previous

168   petrological and phase equilibria studies (Lange and Carmichael 1990; Moore and Carmichael

169   1998), was used as starting material (sample Mas22). The lava is glass-poor (72% vol.

170   groundmass microlites) and encloses phenocrysts of olivine, plagioclase and clinopyroxene.

171   Centimeter-sized subsamples of this lava were crushed coarsely (tens of μm to mm sized

172   particles) to avoid contamination by possibly zoned phenocryst cores. This ensures that only the

173   "reactive" magma participates in the chemical budget of the system, implying that equilibrium

174   should only be partial (i.e., the melt, the newly formed phases and phenocryst rims) (Pichavant et

175   al. 2007). 0.1-0.2 g of starting material was placed into a 5mm OD $Ag_{70}Pd_{30}$ capsule along with

176   enough water to ensure saturation of an H_2O-rich fluid phase upon pressurization (see below).

177   An important assumption (discussed further below) is that Fe was not significantly removed

178   from the melt by reaction with the surrounding AgPd capsule walls.

179

180   Experimental procedure

181

8

182   All experimental charges consisted of the crushed starting material and a CoPd sensor

183   capsule (see below for description of the sensor). In some experiments, pure Fe or Ni oxygen

184   getters (Fe- or Ni-OG, see below) were inserted above the sensor to test whether getters

185   succeeded in maintaining fugacity conditions at steady values. All runs presented here were

186   conducted in the same TZM cold-seal pressure vessel for consistency. Two experiments were

187   also carried out using a molybdenum-halfnium-carbide (MHC) vessel and showed

188   indistinguishable results; another set of experiments were carried out at higher T (1050 and 1075

189   ºC) to test whether the OG was equally effective at conditions favoring faster reaction rates;

190   these sets of experiments are not detailed herein. For all the experiments presented in this paper,

191   conditions of pressure of 150 MPa and a temperature of 1010ºC were chosen based on the phase

192   diagram of Moore and Carmichael (1998) to produce a phase assemblage that includes liquid,

193   plagioclase, clinopyroxene and olivine. About 8-10% wt. H_2O was initially added to the

194   experimental charge to ensure vapor saturation (~4.5% wt. at 150 MPa, based on solubility

195   calculated from Moore et al. 1998). Once the capsule was welded shut and placed at the bottom

196   of the vessel, a graphite filler-rod was inserted which serves two purposes; (1) it ensures that

197   there is no space available for convection within the vessel, which could potentially influence the

198   internal temperature (Boettcher and Kerrick 1971), and (2) it helps maintain reducing redox

199   conditions inside the vessel during the experiment (e.g. Huebner et al. 1971; Matthews et al.

200   2003). It is worth noting that, over time, using filler-rods with compositions different from the

201   vessel may potentially change the structure and thereby the strength of the alloy vessel. Yet an

202   additional worry with metallic filler-rods (Fe, Ni, Co, Ti, W) is the possibility of sintering with

203   the vessel if not properly isolated by Pt spacers (Matthews et al. 2003).

9

204   The temperature of the furnace outside the pressure vessel is accurately controlled by a

205   B-type thermocouple (TC). Because CSPVs do not readily allow for direct measurements of T

206   during high-P runs through additional internal TCs, the temperature requires an indirect

207   calibration (Boettcher and Kerrick 1971); first, the CSPV setup is introduced in the furnace at 1-

208   atm mounted with a K-type TC welded to a coned closure piece. The temperature measured by

209   the K-type TC inside the vessel is thereafter considered to be representative of the sample

210   temperature. Considering that the TC used for calibration has a sensitivity of about ± 2 ºC and

211   that smaller T-variations may occur during the run, we estimate that temperature was constant

212   within ± 5ºC.

213   Total pressure ($P_{TOT}=P_{CH4}+P_{Ar}$) was directly monitored within the pressurized line with a

214   high precision (± 0.007 MPa) Honeywell Sensotec transducer checked against a factory-

215   calibrated 500 MPa Heise bourdon tube fluid gauge for accuracy. After introduction of CH_4 and

216   Ar gases, pressure was rapidly brought to the desired run pressure and the vessel inserted into the

217   furnace. Upon completion of the experiment, the vessel was extracted and forced-air cooled for

218   5-10 s and then plunged into water. The time to reach the glass transition is estimated to be < 15

219   s. This cooling procedure resulted in the formation of quench crystals (≤ 10 μm) in some

220   experiments.

221

222   *f*O_2 sensors: the CoPd-CoO system

223

224   Oxygen fugacity was monitored using solid binary alloy sensors (Taylor et al., 1992).

225   The Co-CoO system was preferred over the Ni-NiO system because it spans a wider range of

226   fugacities (~ NNO-1.5 to NNO+5). A 50-50 mol. % mixture of powdered reagents of Co and Pd

10

227   (> 99.99% purity) were finely ground in acetone, inside an agate mortar, until a fine,

228   homogeneous material was obtained. The resulting CoPd powder was dried and further mixed

229   with ground CoO grains in the molar ratio 3 parts metal/1 part metal oxide. This final CoPd-CoO

230   mixture was then inserted into a 15mm length, 2.4mm OD, 1.6mm ID porous alumina tube

231   capped by a cemented alumina plug 1.6mm in diameter and 1mm in length, and gently

232   compacted into a pellet. The alumina tube was then capped, cemented, and inserted into a 3mm

233   OD Pt capsule. The capsule was welded shut and placed inside the larger capsule containing the

234   starting material (Fig. 1). To test whether the presence of H_2O within the sensor capsule affects

235   the CoPd alloy formation and thus the recorded fO_2, one experiment was performed with H_2O

236   added. The fO_2 calculated from both H_2O-rich and H_2O-poor sensors was indistinguishable (cf.

237   Table 2); as a result, the rest of the sensors were welded shut with no additional water. Because

238   the CoO-CoPd sensor technique was developed at 1-atm (Taylor et al. 1992), we also tested

239   whether pressure could affect the fO_2 calculated from the sensor compositions; a lower

240   temperature (880ºC) experiment was carried out using a horizontal 'clamshell' furnace and a

241   Rene-style waspalloy CPSV pressurized at 200 MPa by water, and using a Ni rod to buffer

242   oxygen fugacity around NNO. The resulting sensor yielded a nearly perfect fO_2 of NNO+0.05,

243   suggesting that pressure has little or no influence on the CoO-CoPd system compared to

244   temperature.

245

246   fO_2 buffers: oxygen getters

247

248   Because fO_2 is expected to increase in the sample capsule during the experiments by

249   dissociation of H_2O and diffusive loss of H_2 through the vessel, simple metal oxygen getters

11

250   (OG) were used in some experiments to test whether fO$_2$ could be maintained at buffer values

251   for longer periods. These OGs serve the same purpose as typical double buffer capsules used in

252   other experiments (e.g., Huebner 1971) but initially contain no metal oxide. Two OGs consisting

253   of high purity (i.e., >99.99%) Fe and Ni reagents were tested. Since intrinsic fO$_2$ of the sample is

254   well above the Iron-Wustite buffer curve, Fe reacts with the environment and captures O$_2$ to

255   form FeO as soon as the experiment is initiated. In the second case, oxidation of Ni begins when

256   fO$_2$ reaches the NNO buffer. The powder of pure metal is inserted into 2.5 mm OD Ag$_{70}$Pd$_{30}$

257   tube with only the bottom crimped and welded (Fig. 1b). If all the available Fe or Ni is exhausted

258   through oxidation, fO$_2$ is no longer maintained near the buffer values, and is expected to

259   increase.

260

261   Variables tested: P$_{CH4}$, t, and OG

262

263   A series of experiments were carried out with variable P$_{CH4}$ (0.3, 0.9, and 1.5 MPa) to

264   evaluate the influence of initial CH$_4$ on the fO$_2$ inside the sample capsule. Next, P$_{CH4}$ was fixed

265   at 0.3 MPa, and time-series runs of 6, 12, 24, 36, 48 and 60 hours were conducted with no OG.

266   In two separate 48 h experiments, CH$_4$ was replenished at t=24h without quenching the charge

267   (i.e., by opening the vessel valve to a pressure line filled with either 0.3 or 5 MPa CH$_4$ and the

268   balance Ar) to examine whether fugacity would remain at more reducing conditions. This

269   procedure is hereafter referred to as 'hot-swapping'. Another longer run (72h) was performed in

270   a similar fashion but with quenching steps at t=24 h and t=48 h, during which the Ar+CH$_4$

271   mixture was purged and replenished with initial values. This practice is hereon referred to as

272   'cold-swapping'. To test whether OGs help maintain fugacity conditions constant, four

12

273   additional experiments (two at t=48h and two at 60h) using Fe or Ni were conducted. Finally,

274   extra H_2O was added to one sensor capsule with the CoPd-CoO mixture, to check whether the

275   water content influenced the evolution of $f O_2$.

276

277   Analytical techniques

278

279   Glass chips, as well as solid cylindrical-shaped sensor rods retrieved from their capsules after

280   quenching were mounted in epoxy for electron microprobe analysis (EMPA). Wavelength-

281   dispersive spectrometry (WDS) analyses of glasses and metal alloys were performed with a

282   JEOL Hyperprobe JXA-8500F at the University of Hawaii. A 15keV acceleration voltage, 10 nA

283   sample current and a defocused 10 μm beam diameter were used for glass analyses. Counting

284   times were: 10 s (Na), 20 s (Si, Al, Ca), 30 s (Fe, Mg, Ti), 40 s (Mn, P), and 50 s (K). Basaltic

285   glass standards VG-2 and A99 (Jarosewich et al. 1980) were repeatedly measured to monitor

286   analytic drift. For the analysis of CoPd alloy compositions, conditions were 20 keV, 30 nA, 5 μm

287   beam diameter, and 30 s counting time. High purity (> 99.99% wt.) Co and Pd metal wires were

288   used for standard calibration. Alloy compositions were also measured with energy-dispersive

289   spectrometry (EDS) to compare with WDS analyses.

290   Experimental phase abundances could not be robustly obtained through mass balance

291   between glass and mineral compositions due to the textural and chemical complexity of the run

292   products (e.g., olivine destabilization in some runs, and pervasive zoning of olivine and

293   clinopyroxene). Instead, phase abundances were determined using backscattered electron (BSE)

294   images. Phases such as olivine, clinopyroxene and oxides were easily distinguished from the

295   glass by applying grayscale thresholds. In contrast, plagioclase crystals were outlined by hand in

13

296   most cases. Because the starting material consists of crushed glass and crystals, fragments or

297   entire phenocrysts from each phase are usually still present after terminating the experiments.

298   Typically, the phases that crystallize during the run are either small individuals within the glass

299   or rims around pre-existing large crystals. In most cases, the newly grown rims show slightly

300   different contrasts within BSE images, allowing discrimination between pre-existing crystalline

301   material from that which formed during the run. It is worth emphasizing that our phase

302   abundance measurements are meaningful only in the context of experiments approaching a state

303   of 'partial' equilibrium (melt with newly formed crystals and phenocryst rims), but not in the

304   context of 'total' equilibrium (the whole system including phenocryst cores) (Pichavant et al.,

305   2007).

306

307   **Results and interpretations**

308

309   Lack of Fe exchange between melt and experimental capsule

310

311   Various studies have reported that Fe from the melt can be lost to the capsule walls (e.g.,

312   Grove, 1981; Gaetani and Grove 1998; Di Carlo et al 2006; Barr and Grove 2010), while others

313   described little to no Fe exchange in their experiments (e.g., Spulber and Rutherford, 1983;

314   Sisson and Grove, 1993; Grove et al. 1997; Parman et al. 1997; Barclay and Carmichael 2004).

315   A potential consequence of Fe loss is the oxidation of the melt via the reaction

316   $FeO_{melt} \leftrightarrow Fe^0_{alloy} + \frac{1}{2}O_2$. To evaluate this possibility, EDS x-ray maps and profiles were

317   performed on a polished capsule from an experiment run for > 48 hours. Although EDS cannot

318   give the same accuracy and precision as EMPA (the detection limit of EDS is 0.2-0.3% wt. for

319   most elements), for simple binary or ternary systems (i.e., AgPd ±Fe) we found that there was

320   little difference between the two techniques (c.f., CoPd analyses in next section). Neither the

321   map nor the profiles revealed the presence of Fe in the capsule material, suggesting that Fe

322   exchange was not significant. In addition, EMPA spots within the rims of experimental glasses,

323   close to the contact between glass and capsule, are indistinguishable from those located in the

324   middle of the glass chip. Thus, it is unlikely that Fe loss to the enclosing capsules was an

325   important factor in the evolution of melt chemistry and thereby fO$_2$ during the experiments.

326

327   CoPd-CoO sensors

328

329   All retrieved sensor cylinders were about 5 mm in length and about 1-1.5 mm in diameter

330   and were coated with a very thin discontinuous bright blue powder. This powder was analyzed

331   and identified as Co-spinel (CoAl$_2$O$_4$), which likely formed as a result of a reaction between the

332   alumina tubing (Al$_2$O$_3$) and the CoO. We consider this reaction to be inconsequential to the

333   formation of the alloy for two reasons; first, the reaction is only very localized on the sensor

334   surface. No Co-spinel is detected in the sensor interior. Second, the removal of some CoO does

335   not affect the capacity of Co and Pd to alloy as fugacity changes (CoO is merely the product of

336   the redox reaction).

337   In BSE images, sensors appear as mixtures of various proportions of grains (CoO) and

338   interconnected blebs of metal (CoPd alloy) (Fig. 2a, b, c, d). Chemical analyses revealed very

339   little spatial variation throughout the sensors (i.e., typically less than 2% wt. variation in the alloy

340   composition, Table 2). In one case where the experimental charge had been clearly corrupted

15

341   (water was lost from a fissured capsule), the sensor contained large chemical variations (up to

342   30% wt changes in Co within the alloy).

343   After analyses of the alloys were obtained, the proportion of Co was converted to fO2

344   using an equation obtained through a combination of formulations by Taylor et al. (1992) and

345   O'Neill and Pownceby (1993):

346

347 $$\log fO_2 = -2\log X_{Co} - \left(\frac{1}{2.3025RT}\right)\left\langle\left(492186 - 509.322T + 53.284T\log T - 0.02518T^2\right) + \left\{2(1 - X_{Co})^2\left[-9.76T + 16445(4X_{Co} - 1)\right]\right\}\right\rangle$$

348   (Equation 1)

349

350   where X_{Co} is the atomic fraction of Co in the CoPd alloy, T is temperature in Kelvins, and

351   R=8.3145 J mol^{-1} K^{-1} is the universal gas constant. Note that the pressure term is absent from this

352   equation since it is inferred to have a negligible effect on the adjusting properties of such metal

353   alloys at crustal-like pressures (Pownceby and O'Neill, 1994). To facilitate the use of Equation

354   1, a calculation spreadsheet is provided in the supplementary material for both Co and Ni-based

355   sensors.

356   Repeat experiments of duration t=24h (same P, T, and amount of CH$_4$ gas in the initial

357   pressurization step) show that the sensors behave very consistently, only showing ~0.03 variation

358   in X_{Co}, which translates into oxygen fugacity uncertainties of about 0.5-0.75 log units. Analyses

359   performed on the same sensors using both EDS and WDS displayed similar values (Table 2),

360   thus EDS was used to perform rapid and accurate quantification for the rest of the sensors. The

361   experiments performed with no extra water within the sensor capsule (i.e., only the ambient

362   humidity, e.g., MAS_fO2_4) and the run carried out with added H$_2$O (MAS_fO2_18) showed no

363   significant difference in calculated fO2 (Table 2).

364

16

365   Effects of varying P_{CH4}

366

367   Three different values of P_{CH4} were tested (0.3, 0.9, 1.5 MPa) corresponding to 0.2, 0.6,

368   and 1% of the total pressure exerted on the charges. After 24h, sensor compositions were

369   X_{Co}=0.3, 0.35, and 0.55 respectively, corresponding to fO_2 values between the FMQ and NNO

370   buffers (Fig. 3a, Table 2). Hence, as expected, higher initial P_{CH4} result in lower initial fO_2. We

371   chose the more oxidized alternative for the time-series experiments (using P_{CH4}=0.3 MPa) to

372   examine oxygen fugacity evolution with time.

373

374   Time-series

375

376   Experiments were quenched at t=6, 12, 24, 36, 48 and 60 h to track the departure of the

377   samples from a hypothetical chemical equilibrium, and monitor changing ambient fO_2 inside the

378   charge using CoPd fO_2 sensors. No oxygen getters were employed in this series.

379   - *Oxygen fugacity*: After 6 hours, the experiments reach the FMQ buffer, at t=24 h they have

380   reached NNO, and after 60 hours, the fO_2 conditions are around NNO+3 (Fig. 3a and 3b). The

381   actual rates of oxidation appear to behave in a log-linear fashion, with values around 1 log

382   unit/12 hours (Fig. 3b). These oxidation rates are much faster than we had hoped, which

383   prompted us to test whether adding oxygen getters to our charges would stabilize fO_2 (see

384   section 4.4 below).

385   - *Phase abundances*: Measured abundances show an increase in overall crystal content and a

386   decrease in glass content (Fig. 4, Table 2). Newly formed plagioclase is the dominant

387   crystallizing phase with an increase from ~9% vol. at t= 6h to ~25% vol. at t= 24h. The

17

388 plagioclase content stays close to the latter value from t= 36h to t= 60h. Olivine shows a similar

389 trend, increasing within runs up to t= 24h and then remaining constant around 3.5% vol until t=

390 48 h. Olivine then nearly disappears after 60 hours of run time. In contrast, clinopyroxene shows

391 a more complex behavior, with two slight increases separated by a decrease in abundance.

392 Finally, Fe-oxides (titanomagnetite) appears in runs >12h and slowly increases in abundance

393 from ~0.8 to 2.4% vol. after 60h. With respect to olivine and plagioclase mode, the data suggest

394 that steady-state crystallinities are approached after about ~20 hrs.

395 - *Olivine destabilization*: In the original lava sample used as initial material as well as in time-

396 series runs quenched at t= 6h and 12 h, olivine phenocrysts appear as very faintly zoned 0.1-0.3

397 mm crystals. In contrast, olivine in runs exceeding 24h displays reaction textures; in BSE

398 images, crystals appear darker and contain planar Fe-oxide lamellae (Fig. 2g, h). Such textures

399 have been described in natural samples (e.g., Stromboli basalts, Cortes et al., 2006) and can

400 develop as a consequence of oxidation. As the valence of Fe changes from 2+ to 3+, olivine

401 rejects iron from its structure, saturating a separate Fe-oxide phase on crystallographically-

402 controlled lattice planes (e.g., Blondes et al., 2012). This impoverishment of Fe^{2+} in olivine is

403 also evidenced by the reduced grayscale intensity of olivines within BSE images. Eventually,

404 after 60 h, olivine almost disappears entirely from the charge.

405 - *Glass chemistry:* Time-series experimental glasses show fairly complex chemical evolutions

406 (Fig. 5, Table 3). Two processes are competing to modify the chemical composition of glasses in

407 the time-series. First and foremost, the mineral compositions and abundances need time to

408 approach equilibrium (primarily through melting and dissolution) at the applied P_{total} and T

409 conditions. Second, the progressive increase in fO_2 acts to shift the equilibrium, stabilizing

18

410   magnetite and destabilizing olivine. Because environmental conditions progressively evolve, the

411   equilibrium state towards which the system evolves is a moving target in these experiments.

412   During the first 12 hours, glass SiO_2 increases while MgO and CaO decrease, and FeO

413   remains constant (Fig. 5). This is consistent with crystallization of plagioclase, and to a lesser

414   extent olivine and clinopyroxene. In longer experiments (t≥ 24h), as the NNO redox conditions

415   are exceeded, compositions shift towards SiO2 enrichment, and FeO, MgO and CaO depletion.

416   Since plagioclase and olivine have mostly stopped growing by t=24h (Fig. 4), these variations

417   must be associated with crystallization of magnetite, and the moderate changes in clinopyroxene

418   abundance. Crystallization of magnetite depletes the melt in FeO, strongly enriches the melt in

419   SiO_2, and only has a minor effect on other elements (Fig. 5). The additional crystallization of

420   clinopyroxene reduces CaO, MgO, FeO. In turn, the destabilization of olivine after ~24 hours is

421   expected to slightly enrich the melt in SiO_2, MgO and FeO, even though newly formed magnetite

422   lamellae probably incorporate substantial Fe released from the olivines. Hence, overall, changes

423   in glass compositions are first dominated by the tendency of the magma to chemically

424   accommodate new pressure-temperature conditions (i.e., from initial glass-poor, crystalline

425   crushed material to crystal-rich melt), and then affected by an upward drift in relative fO_2.

426

427   Effect of OGs

428

429   In view of the fast oxidation occurring within the experimental charges and the

430   consequences for glass chemistry evolution, Fe and Ni were both tested as oxygen getters to

431   stabilize fO_2. The major difference is that as soon as the experiments are started the Fe captures

432   O, whereas Ni begins to seize O only after the NNO buffer curve has been met, ~20-24h into the

19

433   experiment. Thus, for a similar initial amount of OG, Fe will be exhausted earlier than Ni and

434   will not maintain fO_2 stable for the same duration. After 48 h, the sensors record fO_2 values

435   corresponding to NNO+0.7 (OG=Fe) and NNO+0.07 (OG=Ni), compared to ~NNO+2 without

436   an OG (Fig. 3b). Hence, if our purpose is to maintain fO_2 at relatively oxidizing conditions

437   (around NNO), Ni will be better suited than Fe because the total range of fO_2 crossed by the

438   charges is more restricted. In addition, Ni has the advantage of producing a reaction product

439   (NiO) with a characteristic green color, which makes it easy to establish whether the OG worked

440   properly or not. The color can also be used to determine how much Ni is left unoxidized and thus

441   to establish the potential for maintaining fO_2 stable in even longer subsequent experiments. To

442   this end, two 60 h runs were performed using different amounts of Ni in the OG. In both cases,

443   the sensors record values around NNO+1.5, implying that OGs become less efficient in

444   maintaining fO_2 at t> 48 h. The use of Ni as an OG maintains constant phase abundances, except

445   for olivine which appears to decrease at t> 48 h in experiments with and without OG (Fig. 4).

446   The presence of OGs also improves the range in glass composition traversed, reducing the

447   increase in SiO_2, and the decrease in FeO attributed to the prolonged crystallization of magnetite

448   (Fig. 5).

449

450   Effect of replenishment

451

452   Different strategies were employed to establish whether injecting more CH_4 into the

453   pressure line would help mitigate fast oxidation; the 48 h experiment MAS_fO2_8 performed

454   with a 0.3 MPa CH_4 (+Ar) hot gas-swap at t=24 h shows the same fO_2 conditions than a normal

455   48 h experiment with no gas replenishment (ΔNNO ~ +1.5 2). A similar experiment involving a

20

456 replenishment step using more methane (P_{CH4}=5MPa, MAS_fO_2_17) showed an improvement

457 compared to the other 48 h runs (i.e., ΔNNO = +0.7). The other strategy consisted in performing

458 cold-swaps every 24 h prior to replenishment with pressurizing gases. The resulting 72 h

459 experiment (MAS_fO_2_9) experienced a significantly more reduced environment (ΔNNO = -1).

460 Overall, these various sets of experiments show that while replenishment techniques can

461 maintain fO_2 around NNO at durations of 72 h, more absolute variability is to be expected.

462

463 **Discussion**

464

465 These results have important consequences for experimental investigations of hydrous

466 mafic systems at high temperature. The consequences of not maintaining stable fO_2 are

467 considered, along with implication for achieving thermodynamic equilibrium in CSPV

468 experiments. An important preamble to this discussion is that our experimental results involve a

469 specific composition at fixed P-T conditions, carried out within a specific laboratory setup.

470 Considering that the type of CSPV (i.e., TZM or MHC), sheath and furnace setups, line volumes

471 and materials employed may vary, we stress that oxygen fugacity may evolve at a different rate

472 in different apparatus. Hence, investigators should be cautious about extrapolating our fO_2

473 conditions directly.

474

475 The challenges of maintaining stable oxygen fugacity

476

477 Experiments performed in CSPV show that oxygen fugacity conditions are not constant

478 during runs. While the quantity of CH$_4$ added to the initial pressure system shifts the

21

479   experimental fO_2 to higher or lower values (Fig. 2a), it does not affect the rate at which

480   oxidation occurs. Instead, our time-series reveals that fO_2 increases by 3-4 orders of magnitude

481   in just 48h. This is particularly problematic for experimental runs that require equilibration times

482   longer than just a few hours (e.g., Berndt et al. 2005). The use of OG such as Ni to capture O and

483   counterbalance the diffusion of H_2 outside the capsule helps stabilize and maintain fO_2 to

484   relatively constant values. In our runs, all OG capsules still contained unoxidized Ni powder

485   (<1/2 the initial amount, 0.06g), suggesting that fO_2 can be maintained for longer than 48h, but

486   not realistically for much longer. A 60h experiment (MAS_fO2_15, Table 2) shows that even

487   with more Ni added to the initial setup, fO_2 is ~1.5 log units above the desired NNO buffer

488   value. Potentially, after a certain time, the limiting factor is not the abundance of oxygen that can

489   be captured by the OG, but rather the depletion of hydrogen in the capsule and vessel. For

490   experiments of up to 72 h, the runs can undergo hot- or cold-swapping, with CH_4 being re-

491   injected every 24 h. This proved to be the only means of stabilizing fO_2 around NNO for over 48

492   h (Table 2).

493

494   Consequences of fast oxidation

495

496   Rapid changes in redox conditions affect the valence state of elements, particularly Fe in

497   magmas, and modify minerals and the host-melt in various ways.

498   - *Stabilization of Fe-oxides*: One of the major consequences of increasing fO_2 in melts is the

499   crystallization of oxide phases such as magnetite (Fe_3O_4) that readily acquire the available Fe^{3+}

500   (e.g., Osborn 1959; Toplis and Carroll 1995). This phenomenon was observed in our time-series,

501   after about ~20h when fO_2 attains NNO, and led to an increase in melt SiO_2 (from ~57 to

22

502   ~59.5% wt., Fig. 5) accompanied by a decrease in FeO (from 6 to about 3.5% wt.). Over-

503   production of magnetite, essentially due to an experimental artifact, can cause unwanted and

504   profound deviations from natural crystallization sequences. For example, Fe-depletion from the

505   melt at high fO_2 could cause the melt to inadvertently shift from a tholeiitic to a calc-alkaline

506   magma differentiation trend (e.g., Berndt et al. 2005; Hammer 2006). Second, because Fe-

507   bearing oxides and clinopyroxenes crystallize epitaxially (Hammer 2010), the presence of

508   magnetite could stabilize clinopyroxene earlier during the melt's evolution than would otherwise

509   occur.

510   - *Destabilization of olivine*: mafic minerals such as olivine (and orthopyroxene) preferentially

511   incorporate Fe^{2+} over Fe^{3+} into their structure (e.g. Nakamura and Schmalzried 1983). Hence, as

512   fO_2 increase and the valence of Fe changes, olivine releases Fe, which then forms exsolution

513   lamellae of magnetite according to the reaction:

514

515     $3Fe_2SiO_4^{Ol} + O_2 \rightarrow 2Fe_3O_4^{Mt} + 3SiO_2^{Liq}$
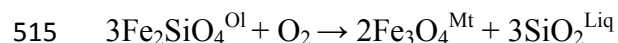
516

517   As a result, olivines destabilize and the residual olivines evolve towards more forsteritic

518   compositions (e.g., Muan, 1958; Osborn, 1959; Cortes et al., 2006; Blondes et al., 2012 and

519   references therein) (see Fig. 2). The dissolution of olivine along crystallographic planes and the

520   ensuing percolation of melt outward into the matrix automatically cause olivine cores initially far

521   from the melt to be in contact and possibly re-equilibrate. This effect can have deleterious effects

522   in circumstances where Mg/Fe partition coefficients K_D compositions are used to establish

523   equilibrium. The compositional effect on the surrounding melt in our series is expected to be

524   fairly minimal at first, since oxides incorporate the Fe released from destabilizing olivines (t=24-

23

525   48 h), and then more pronounced as entire crystals dissolve (t > 48 h, Figure 4); this decrease in

526   olivine abundance after 48h is accompanied by slight increases in melt MgO (Figure 5). In

527   contrast, the distribution coefficient D_{SiO2} between olivine and melt is close enough to unity, that

528   it is difficult for small changes in olivine abundance to greatly change the melt's SiO_2

529   concentration.

530   *- Effects on other phases*: In contrast with olivine, plagioclase preferably includes Fe^{3+} and can

531   be used as a geobarometer (e.g., Sugarawa, 2001). Even though plagioclase is the dominant

532   mineral in the present experiments (~25% vol., Figure 4), it only admits up to 0.75-0.90% FeO

533   (c.f., Moore and Carmichael 1998 for plagioclase analysis). Thus, the uptake of Fe^{3+} by

534   plagioclase should not affect the melt composition markedly. However, clinopyroxene readily

535   incorporates both Fe^{2+} and Fe^{3+}, a property employed in geobarometry (Luth and Canil 1993;

536   McCanta et al. 2004). Matrix glass compositions of the time-series experiments indicate that

537   pyroxene continues to form even after most other phase abundances have stabilized (Figure 4).

538   This has a non-negligible effect on melt composition, primarily a decrease in MgO and CaO

539   (Fig. 5). Since clinopyroxene is capable of incorporating larger amounts of Fe^{3+} under oxidizing

540   conditions (McCanta et al. 2004), progressive oxidation could aid in stabilizing additional

541   clinopyroxene (Toplis and Carroll 1995).

542

543   Assessment of progress toward chemical equilibrium

544

545   Phase equilibria, or so-called "static" experiments performed at constant P and T conditions,

546   commonly use crushed starting material or glass previously fused at superliquidus conditions

547   (Pichavant et al. 2007; Hammer 2008 and references therein). In the first case, equilibrium is

24

548 approached dominantly by melting/dissolution, and in the second, by crystallization. In both

549 cases, it is expected that phases will either dissolve or crystallize until a partial thermodynamic

550 equilibrium is approached (e.g., Edgar et al. 1973). One or more lines of evidence may be

551 employed to demonstrate that the run time was sufficient for the system to closely approach

552 equilibrium (Fyfe 1960; Edgar 1973; Grove and Bence 1979; Sisson and Grove 1993; Pichavant

553 et al. 2007; Hammer 2008):

554 - *Comparisons with experimental timescales of previous investigations* that used similar

555   compositions of reactive magma (e.g., Di Carlo et al. 2006; Feig et al. 2010).

556 - *Idiomorphic crystal morphologies* are assumed to show that phases were crystallizing and

557   not in the process of dissolving (e.g., Toplis and Carroll 1995; Moore and Carmichael

558   1998; Di Carlo et al. 2006; Feig et al. 2010).

559 - *Chemical homogeneity of crystal and glass phases* of the reactive magma (e.g., Toplis an

560   Carroll, 1995; Moore and Carmichael 1998; Berndt et al. 2005; Di Carlo et al. 2006; Feig

561   et al. 2010).

562 - Time-independence of *phase compositions* (e.g. Metrich and Rutherford 1998; Gaillard et

563   al. 2002; Berndt et al. 2005).

564 - Time independence of *type and abundance of phases* (though the crystal numbers and

565   sizes can change through textural maturation) (e.g., Berndt et al. 2005).

566 - Similar phase abundances and composition in runs performed from *both the*

567   *crystallization and melting/dissolution* sides (i.e., reversals) (e.g., Toplis and Carroll

568   1995; Moore et al. 1995; Hammer et al. 2002; Berndt et al. 2005).

25

569   -   Equilibrium value of *exchange coefficients* for specific elements in the melt and minerals

570   (i.e., partition of Fe, Mg in olivine and melt) (e.g., Grove and Bence 1979; Toplis and

571   Carroll 2005; Di Carlo et al. 2006).

572

573   Our experiments utilized natural, holocrystalline lava, to approach an equilibrium state that

574 includes a melt phase. Thus, in terms of phase mode, it could be inferred that equilibrium was

575 approached primarly by solid dissolution. However, crystal abundances in the shortest run were

576 minima, with mineral abundances reaching plateaus after 20-24h (Fig. 4). Furthermore,

577 idiomorphic crystal shapes suggest that crystals were growing and not dissolving. Most likely,

578 processes of coarsening and ripening (e.g., Park and Hanson 1999; Cabane et al. 2005) are

579 responsible for the presence of faceted morphologies in most phases, and satisfactorily explain

580 an approach to equilibrium by crystallization in our experiments.

581   Out of the indicators of equilibrium listed above, those that demonstrate time independence

582 of phase abundances and chemistry are probably the most robust (Fyfe 1960; Edgar 1973 and

583 references therein). Phase abundances are, however, most often estimated using mass balance

584 calculations (e.g., Albarede 1977), and seldom assessed independently from glass or crystal

585 compositions. For our runs, phase proportions were measured using 2D BSE images separately

586 from compositions. Our independent assessments suggest that while time-invariance is a valid

587 assessment of phase abundances after ~20-24h (glass, plagioclase, olivine, Fig. 4), glass

588 compositions (Fig. 5) vary throughout the entire experimental timescale. As described above,

589 oxidation is the likely culprit for both changing glass compositions and phase abundances

590 (particularly magnetite, olivine and clinopyroxene). We conclude that chemical equilibrium

591 would be impossible to demonstrate from the compositions of phases in CSPV experiments in

592 which oxidation proceeds at the high rates we observe. Furthermore, the near complete

593 dissolution of olivine after 60 hours violates the premise that phenocryst interiors do not form

594 part of the reactive magma; while the effects of olivine destabilization on the melt composition

595 are rather moderate in our series, the same cannot be expected of experiments that may have

596 higher olivine abundances to begin with. Fortunately, these effects can be mitigated by inclusion

597 of the Ni-OG in an experimental charge, stabilizing the glass composition for 24-48 h (Fig. 5).

598 For runs requiring longer equilibration timescales (e.g., more felsic and/or colder magmas),

599 charges need to be hot- or cold-swapped every ~24-48 hours to maintain the magma near

600 chemical equilibrium.

601

602 Applicable experimental durations and solutions for longer experiments

603

604 Since the rates of oxygen fugacity increase with time depends strongly on temperature (e.g.,

605 Hewitt 1978), we can expect that fO$_2$ in hotter experiments (i.e., T > 1010°C) will be difficult to

606 keep constant for more than 2 days (whereas cooler experiments can be kept at fixed conditions

607 for longer durations). Hence, realistically, static phase equilibria runs at high T can be performed

608 up to durations of about 96 h (counting one step of quenching-replenishment), whereas dynamic

609 experiments involving decompression or cooling may be limited to a maximum of 48 h

610 (considering that quench-replenishment steps may interfere with the changing P or T conditions).

611 Fortunately, because the rates of chemical diffusion in the melt phase are fast within hotter mafic

612 magmas (e.g., Watson 1994), timescales of 48-96h are sufficient for a wide range of applications

613 to simulate natural systems. In fact, most static and dynamic experiments involving mafic

614 compositions are typically performed within timescales < 96 h (c.f., Table 1 and references

27

615 therein), because these durations are deemed sufficient for such systems to reach steady-states. In

616 natural systems involving mafic magmas, the rates of magmatic ascent are thought to be fast

617 during both effusive and explosive eruptions (0.03-30 m/s, Klein 1987; Rutherford 2008). For

618 instance, assuming a lithostatic pressure gradient with a wallrock density ρ=2500 kg m^{-3}, a total

619 decompression of 100 MPa from the storage to the fragmentation level (or the free magma

620 surface for effusive eruptions) within an experimental timeframe of 48 h allows for ascent rates

621 as low as ~0.024 m/s. Similarly, for a total cooling of 100-150°C, cooling rates as low as 2-

622 3°C/hour can be applied. Therefore, overall, total durations of 48-96 hours are adequate to

623 simulate a large range of natural magmatic processes typical of mafic systems.

624 Nonetheless, there are cases where investigators will need to perform much longer

625 experiments to characterize slower processes (e.g., experiments initiated near a phase boundary

626 where transformation rates are slow, crystal ripening experiments, etc.) In such cases, alternative

627 setups allowing experimentalists to perform runs without the burdensome steps of quenching and

628 re-pressurization should be considered. The only suitable method to impose and maintain fO$_2$ in

629 long-duration experiments involving hot mafic magmas is the Shaw-membrane technique. While

630 it requires modifications to the CSPV setup and additional safety precautions associated with H$_2$,

631 gas, it potentially allows fO$_2$ to be maintained fixed throughout an experiment for durations

632 longer than 48 h (Scaillet et al. 1992).

633

634

28

641

642   References

643   Barclay, J. and Carmichael, I.S.E. (2004) A hornblende basalt from Western Mexico: water-

644   saturated phase relations constrain a pressure-temperature window of eruptibility. Journal of

645   Petrology, 45, 485–506.

646   Barr, J.A., Grove, T.L. and Wilson, A.H. (2009) Hydrous komatiites from Commondale, South

647   Africa: an experimental study. Earth and Planetary Science Letters, 284, 199–207.

648   Barr, J.A. and Grove, T.L. (2010) AuPdFe ternary solution model and applicatiosn to

649   understanding the fO2 of hydrous, high-pressure experiments. Contributions to Mineralogy and

650   Petrology, 160, 631–643.

651   Berndt, J., Koepke, J. and Holtz, F. (2005) An experimental investigation of the influence of

652   water and oxygen fugacity on differentiation of MORB at 200 MPa. Journal of Petrology, 46,

653   135–167.

654   Blondes, M.S., Brandon, M.T., Reiners, P.W., Zeb Page, F., Kita, N.T. (2012) Generation of

655   forsteritic olivine ($Fo_{99.8}$) by subsolidus oxidation in basaltic flows. Journal of Petrology, 53,

656   971–984.

657   Blundy, J. and Cashman, K.V. (2008) Petrologic reconstruction of magmatic system variables

658   and processes. Reviews in Mineralogy and Geochemistry, 69, 179–239.

29

659 Boettcher, A.L. and Kerrick, D.M. (1971) Temperature calibration in cold-seal pressure vessels.

660 In Ulmer GC (ed), Research techniques for high pressure and high temperature, Springer-Verlag,

661 New York, pp 174–181.

662 Cabane, H., Laporte, D. and Provost, A. (2005) An experimental study of Ostwald ripening of

663 olivine and plagioclase in silicate melts : implications for the growth and size of crystals in

664 magmas. Contributions to Mineralogy and Petrology, 150, 37–53.

665 Carmichael, I.S.E. and Nicholls, J. (1967) Iron-titanium oxides and oxygen fugacities in volcanic

666 rocks. Journal of Geophysical Research, 72, 4665–4687. doi:10.1029/JZ072i018p04665.

667 Carmichael, I.S.E. and Ghiorso, M.S. (1990) The effect of oxygen fugacity on the redox state of

668 natural liquids and their crystallizing phases. Reviews in Mineralogy and Geochemistry, 24,

669 191–212.

670 Carmichael, I.S.E. (1991) The redox state of basic and silicic magmas: a reflection of their

671 source regions? Contributions to Mineralogy and Petrology, 106, 129–141.

672 Coombs, M.L., Eichelberger, J.E. and Rutherford, M.J. (2000) Magma mixing and storage

673 conditions for the 1953-1974 eruptions of Southwest Trident volcano, Katmai National Park,

674 Alaska. Contributions to Mineralogy and Petrology, 140, 99–118.

675 Cortes, J.A., Wilson, M., Condliffe, E. and Francalanci, L. (2006) The occurrence of forsterite

676 and highly oxidizing conditions in basaltic lavas from Stromboli volcano, Italy. Journal of

677 Petrology, 47, 1345–1373.

30

678 Dann, J.C., Holzheid, A.H., Grove, T.L. and McSween, H.Y. (2001) Phase equilibria of the
679 Shergotty meteorite: constraints on pre-eruptive water contents of martian magmas and fractional
680 crystallization under hydrous conditions. Meteoritics Planetary Science, 36, 793–806.

681 Di Carlo, I., Pichavant, M., Rotolo, S.G. and Scaillet, B. (2006) Experimental crystallization of a
682 high-K arc basalt: the golden pumice, Stromboli volcano (Italy). Journal of Petrology, 47, 1317–
683 1343.

684 Di Traglia, F., Cimarelli, C., de Rita, D. and Gimeno Torrente, D. (2009) Changing eruptive
685 styles in basaltic explosive volcanism: examples from Croscat complex scoria cone, Garrotxa
686 Volcanic Field (NE Iberian Peninsula). Journal of Volcanology and Geothermal Research, 180,
687 89–109.

688 Edgar, A.D. (1973) Experimental petrology-Basic principles and techniques. Oxford University
689 Press, New York

690 Eugster, H.P. (1957) Heterogeneous reactions involving oxidation and reduction at high
691 pressures and temperatures. Journal of Chemistry and Physics, 26, 1760–1761.

692 Feig, S.T., Koepke, J. and Snow, J.E. (2010) Effect of oxygen fugacity and water on phase
693 equilibria of a hydrous tholeiitic basalt. Contributions to Mineralogy and Petrology, 160, 551–
694 568.

695 Frantz, J.D. and Eugster, H.P. (1973) Acid-base buffers: use of Ag + AgCl in the experimental
696 control of solution equilibria at elevated pressure and temperatures. American Journal of
697 Science, 273, 269–296.

31

698   Fyfe, W.S. (1960) Hydrothermal Synthesis and Determination of Equilibrium between Minerals

699   in the Subliquidus Region. Journal of Geology, 68, 553–566.

700   Gaetani, G.A., Grove, T.L. and Bryan, W.B. (1994) Experimental phase relations of basaltic

701   andesite from hole 839B under hydrous and anhydrous conditions. Proceedings of the Ocean

702   Drilling Program: Scientific Results, 135, 557–563.

703   Gaetani, G.A. and Grove, T.L. (1998) The influence of water on melting of peridotite.

704   Contributions to Mineralogy and Petrology, 131, 323–346.

705   Gaillard, F., Scaillet, B. and Pichavant, M. (2002) Kinetics of oxidation-reduction in hydrous

706   silicic melts. American Mineralogist, 87, 829–837.

707   Gardner, J.E., Rutherford, M.J., Carey, S. and Sigurdsson, H. (1995) Experimental constraints on

708   pre-eruptive water contents and changing magma storage prior to the explosive eruptions of Mt.

709   St. Helens volcano. Bulletin of Volcanology, 57, 1–17.

710   Grove, T.L. and Bence, A.E. (1979) Crystallization kinetics in a multiply saturated basalt

711   magma, An experimental study of Luna 24 ferrobasalt. Proceedings of the 10th Lunar Science

712   Conference, 10, 439–478.

713   Grove, T.L. (1981) Use of FePt alloys to eliminate the iron loss problem in 1 atmosphere gas

714   mixing melting experiments: theoretical and practical considerations. Contributions to

715   Mineralogy and Petrology, 78, 298–304.

716   Grove, T.L., Donnelly-Nolan, J.M. and Housh, T. (1997) Magmatic processes that generated the

717   rhyolite of Glass Mountain, Medicine Lake Volcano, N. California. Contributions to Mineralogy

718   and Petrology, 127, 205–223.

719   Gunter, W.D., Myers, J. and Girsperger, S. (1987) Hydrogen, metal membranes. In: Ulmer GC,

720   Barnes HL (eds) Hydrothermal Experimental Techniques, John Wiley & Sons, New York, pp

721   100–120.

722   Hammer, J.E., Rutherford, M.J. and Hildreth, W. (2002) Magma storage prior to the 1912

723   eruption at Novarupta, Alaska. Contributions to Mineralogy and Petrology, 144, 144–162.

724   Hammer, J.E. (2006) Influence of fO2 and cooling rate on the kinetics and energetics of Fe-rich

725   basalt   crystallization.   Earth   and   Planetary   Science   Letters,   248,   618–637.   doi

726   10.1016/j.epsl.2006.04.022

727   Hammer, J.E. (2008) Experimental studies of the kinetics and energetics of magma

728   crystallization. Reviews in Mineralogy and Geochemistry, 69, 9–59.

729   Holloway, J.R. (1971) Internally-heated pressure vessels. In Ulmer GC (ed) Research techniques

730   for high pressure and high temperature, Springer-Verlag, New York, pp 217–258.

731   Holloway, J.R. and Wood, B.J. (1988) Simulating the Earth: Experimental geochemistry, Unwin

732   Hyman, Massachusetts.

733   Houghton, B.F. and Gonnerman, H.M. (2008) Basaltic explosive volcanism: constraints from

734   deposits and models. Chemie der Erde, 2, 117–140.

735   Huebner, J.S. (1971) Buffering techniques for hydrostatic systems at elevated pressures. In

736   Ulmer GC (ed) Research techniques for high pressure and high temperature, Springer-Verlag,

737   New York, pp 123–178.

33

738   Huebner, J.S. (1987) Use of gas mixtures at low pressure to specify oxygen and other fugacities

739   of furnace atmospheres. In: Ulmer GC, Barnes HL (eds) Hydrothermal Experimental

740   Techniques, John Wiley & Sons, New York, pp 20–60.

741   Jarosewich, E., Nelen, J.A. and Norberg, J.A. (1980) Reference Samples for Electron

742   Microprobe Analysis. Geostandards Newsletter, 4, 43–47.

743   Kerrick, D.M. (1987) Cold-seal systems. In: Ulmer GC, Barnes HL (eds) Hydrothermal

744   Experimental Techniques, John Wiley & Sons, New York, pp 293–323.

745   Klein, F.W., Koyanagi, R.Y., Nakata, J.S. and Tanigawa, W.R. (1987) The seismicity of

746   Kilauea's magma system. US Geological Survey Professional Paper, 1350, 1019–1185.

747   Kouchi, A. and Sunagawa, I. (1983) Mixing basaltic and dacitic magmas by forced convection.

748   Nature, 304, 527–528.

749   Lofgren, G. (1987) Internally heated systems. In: Ulmer GC, Barnes HL (eds) Hydrothermal

750   Experimental Techniques, John Wiley & Sons, New York, pp 325–332.

751   Matthews, W., Linnen, R.L. and Guo, Q. (2003) A filler-rod technique for controlling redox

752   conditions in cold-seal-pressure vessels. American Mineralogist, 88, 701–707.

753   McCanta, M.C., Darby Dyar, M., Rutherford, M.J. and Delaney, J.S. (2004) Iron partitioning

754   between basaltic melts and clinopyroxene as a function of oxygen fugacity. American

755   Mineralogist, 89, 1685–1693.

756   Métrich, N. and Rutherford, M.J. (1998) Low pressure crystallization paths of H2O-saturated

757   basaltic-hawaiitic melts from Mt Etna: implications for open-system degassing of basaltic

758   volcanoes. Geochimica Cosmochimica Acta, 62, 1195–1205.

34

759   Moore, G., Righter, K. and Carmichael, I.S.E. (1995) The effect of dissolved water on the

760   oxidation state of iron in natural silicate liquids. Contributions to Mineralogy and Petrology 120,

761   170–179.

762   Moore, G. and Carmichael, I.S.E. (1998) The hydrous phase equilibria (to 3 kbar) of an andesite

763   and basaltic andesite from western Mexico: constraints on water content and conditions of

764   phenocryst growth. Contributions to Mineralogy and Petrology 130, 304–319.

765   Moore, G., Vennemann, T. and Carmichael, I.S.E. (1998) An empirical model for the solubility

766   of H2O in magmas to 3 kilobars. American Mineralogist 83, 36–42.

767   Muncill, G.E. and Lasaga, A.C. (1988) Crystal-growth kinetics of plagioclase in igneous

768   systems: Isothermal H2O-saturated experiments and extension of a growth model to complex

769   silicate melts. American Mineralogist, 73, 982–992.

770   Muan, A. (1958) Phase equilibria at high temperature in oxide systems involving changes in

771   oxidation states. American Journal of Science, 256, 171–207.

772   Mysen, B.O. (2006) Redox equilibria of iron and silicate melt structure: Implications for

773   olivine/melt element partitioning. Geochimica Cosmochimica Acta, 70, 3121–3138.

774   Nafziger, R.H. (1971) Gaseous buffering for the control of oxygen fugacity at one atmosphere.

775   In Ulmer GC (ed) Research techniques for high pressure and high temperature, Springer-Verlag,

776   New York, pp 9–42.

777   Nakamura, A. and Schmalzried, H. (1983) On the stoichiometry and point defects of olivine.

778   Physics and Chemistry of Minerals, 23, 345–353.

35

779 O'Neill, H.S.C. and Pownceby, M.I. (1993) Thermodynamic data from redox reactions at high

780 temperatures. I. An experimental and theoretical assessment of the electrochemical method using

781 stabilized zirconia electrolytes, with revised values for the Fe-"FeO", Co-CoO, Ni-NiO and Cu-

782 Cu2O oxygen buffers, and new data for the W-WO2 buffer. Contributions to Mineralogy and

783 Petrology, 114, 296–314.

784 Osborn, E.F. (1959) Role of oxygen pressure in the crystallization and differentiation of basaltic

785 magma. American Journal of Science, 257, 609–647.

786 Park, Y. and Hanson, B. (1999) Experimental investigations of Ostwald-ripening rates of

787 forsterite in the haplobasaltic system. Journal of Volcanology and Geothermal Research, 90,

788 103–113.

789 Parman, S.W., Dann, J.C., Grove, T.L. and de Wit, M.J. (1997) Emplacement conditions of

790 komatiite magmas from the 3.49 Ga Komati formation, Barberton greenstone belt, South Africa.

791 Earth and Planetary Science Letters, 150, 303–323.

792 Pichavant, M., Martel, C., Bourdier, J-L. and Scaillet, B. (2002) Physical conditions, structure,

793 and dynamics of a zoned magma chamber: Mount Pelee (Martinique, Lesser Antilles arc).

794 Journal of Geophysical Research, 107, B52093

795 Pichavant, M., Costa, F., Burgisser, A., Scaillet, B., Martel, C. and Poussineau, S. (2007)

796 Equilibration scales in silicic to intermediate magmas: Implications for experimental studies.

797 Journal of Petrology, 48, 1955–1972.

798 Pownceby, M.I. and O'Neill, H.S.C. (1994) Thermodynamic data from redox reactions at high

799 temperatures. III. Activity-composition relations in Ni-Pd alloys from EMF measurements at

800   850-1250 K, and calibration of the NiO + Ni-Pd assemblage as a redox sensor. Contributions to

801   Mineralogy and Petrology, 116, 327–339.

802   Rutherford, M.J. (2008) Magma ascent rates. Reviews in Mineralogy and Geochemistry, 69,

803   241-271.

804   Scaillet, B., Pichavant, M., Roux, J., Humbert, G. and Lefèvre, A. (1992) Improvements of the

805   Shaw membrane technique for measurement and control of fH2 at high temperatures and

806   pressure. American Mineralogist, 77, 647–655.

807   Schmidt B., Scaillet B., Holtz F. (1995): Accurate control of fH_2 in cold-seal pressure vessels

808   with the Shaw membrane technique, European Journal of Mineralogy, 7, 893-903.

809   Shaw, H.R. (1963) Hydrogen-vapor mixtures; control of hydrothermal experiments by hydrogen

810   osmosis. Science, 139, 1220–1222.

811   Simakin, A.G., Salova, T.P. and Babansky, A.D. (2009) Amphibole crystallization from a water-

812   saturated andesite melt: experimental data at P=2kbar. Petrology, 17, 591–605.

813   Sisson, T.W. and Grove, T.L. (1993) Experimental investigations of the role of H_2O in calc-

814   alkaline differentiation and subduction zone magmatism. Contributions to Mineralogy and

815   Petrology, 113, 143–166.

816   Spulber, S., Rutherford, M.J. (1983) The origin of rhyolite and plagiogranite in oceanic crust: an

817   experimental study. Journal of Petrology, 24, 1–25.

818   Sugawara, T. (2001) Ferric iron partitioning between plagioclase and silicate liquid:

819   thermodynamics and petrologicaly applications. Contributions to Mineralogy and Petrology, 141,

820   659–686.

37

821   Taylor, J.R., Wall, V.J. and Pownceby, M.I. (1992) The calibration and application of accurate

822   redox sensors. American Mineralogist, 77, 284–295.

823   Toplis, M.J. and Carroll, M.R. (1995) An experimental study of the influence of oxygen fugacity

824   on Fe-Ti oxide stability, phase Relations, and mineral-melt equilibria in ferro-basaltic systems.

825   Journal of Petrology, 36, 1137–1170.

826   Ulmer, G.C. (1971) Research Techniques for High Pressure and High Temperature. Springer-

827   Verlag, Berlin-Heidelberg-New York.

828

829   **Captions**

830

831   **Figure 1.** (a) Simplified box-sketch of the various components and reactions that are found in the

832   CSPV experiments described herein. The largest bounding box represents the cold-seal TZM

833   pressure vessel, which is pressurized using a mixture of argon and methane. The outer capsule

834   containing the experimental charge is welded, and only hydrogen can diffuse in or out. (b)

835   Specific setup used for experimental charges. The crushed starting material is placed at the

836   bottom along with enough H2O to saturate the melt. The CoPd sensor capsule and the Ni or Fe

837   oxygen getter are inserted on top, with the getter being only welded shut at the bottom to allow

838   oxygen to circulate and react with the Ni or Fe. The sensor capsule is welded shut on both ends

839   to only let hydrogen diffuse in and out.

840

841   **Figure 2**. BSE images of selected oxidation experiments. (a) to (d), retrieved CoPd-CoO oxygen

842   fugacity sensors for different initial partial pressures of methane (a and b), and different run

38

843   times (b and c). (d) A close-up of (c) shows the interconnected blebs of CoPd alloy (white)

844   surrounded by patches of CoO (grey porous grains). (e) to (f), images of experimental glasses

845   retrieved with the sensors. (e) At P_{CH4}=1.5 MPa, the charge contains zoned olivine and

846   clinopyroxene phenocrysts, with plagioclase being hardly distinguishable from the glass. (f) At

847   lower P_{CH4}=0.3 MPa, the run experiences higher fO_2 which permits stabilization of tiny oxides

848   in the groundmass. (g) and a close-up (h) show a run at similar P_{CH4} after 48 h, in which olivine

849   has started to destabilize into magnetite and SiO_2 (melt). Note the crystallographic orientation of

850   destabilization lamellae of magnetite along the olivine structure.

851

852   **Figure 3**. (a) fO_2 variations for experiments of various durations as monitored by X_{Co}, the cobalt

853   fraction of the CoPd alloy. The thick red curve for the CoO-CoPd system is obtained through the

854   equation defined in the main text. Through measurements of X_{Co}, the oxygen fugacity conditions

855   can be calculated. The inset illustrates how fO_2 calculated after a 24h run can be modulated by

856   varying the amount of CH_4 initially injected along with Ar to pressurize the vessel. (b) $fO2$

857   variations against experimental duration for charges containing no oxygen getter (labeled 'no

858   OG') and charges containing Ni and Fe as OG. For runs of up to 48h, the range in $fO2$ traversed

859   by the experiments can be nearly halved by inserting a Ni OG within the experimental capsule.

860

861   **Figure 4**. Phase abundances measured from BSE images for time-series experiments.

862

863   **Figure 5**. Major element glass chemistry plots for SiO_2, FeO, CaO and MgO. Thick gray

864   horizontal lines represent the average glass composition at t=24h. Triangles in the lower right

865   insets show the magnitude of compositional change for addition of 2% volume of a given phase.

Reactions:

① $H_2O = H_2 + 1/2\,O_2$

② $xCo(1\text{-}x)Pd + 1/2yO_2 = Co_zPd_{(1\text{-}x)} + Co_{(1\text{-}z)}O_y$

③ $Metal + 1/2O_2 = Metal\ Oxide$
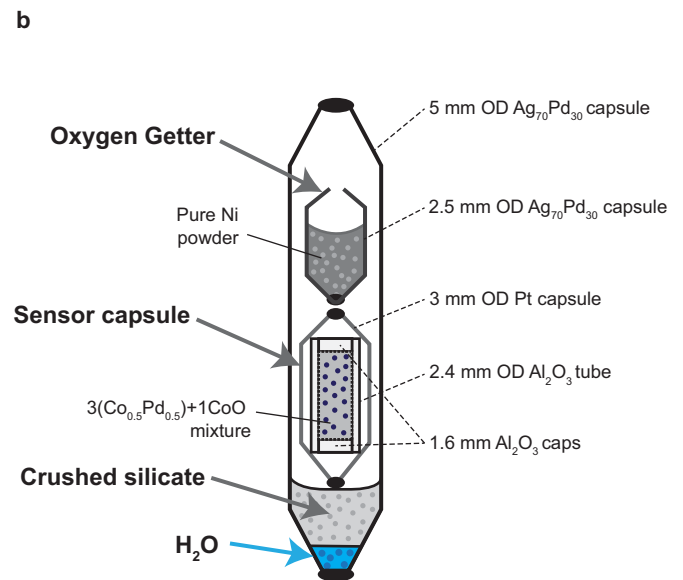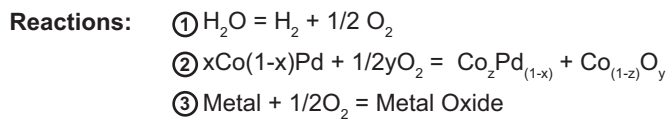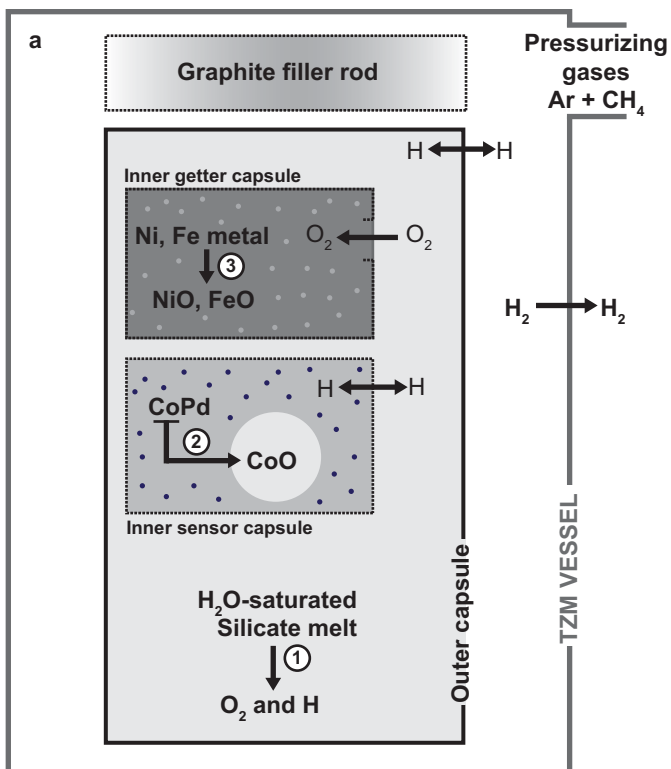
t = 24 h, P_{CH4} = 1.5 MPa

t = 24 h, P_{CH4} = 0.3 MPa

t = 48 h, P_{CH4} = 0.3 MPa

Close-up of c

SiO_2 = 56.47% wt.   Mg# = 0.40

SiO_2 = 56.86 % wt.   Mg# = 0.35

SiO_2 = 59.32 % wt.   Mg# = 0.46
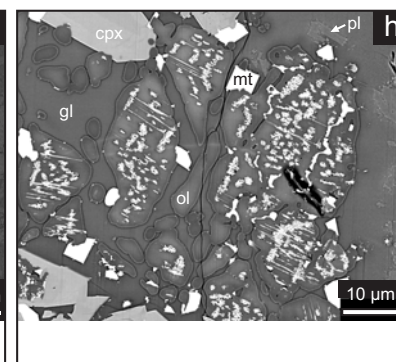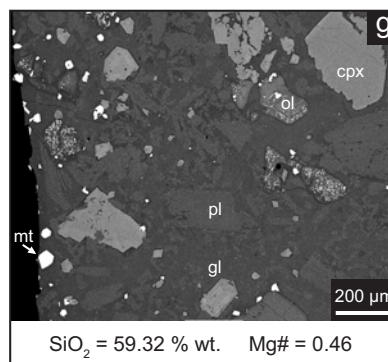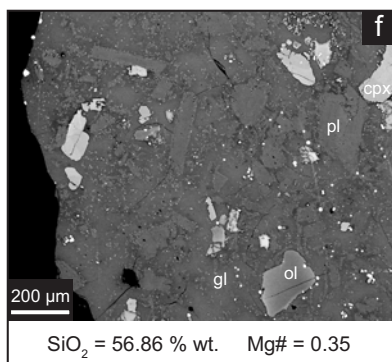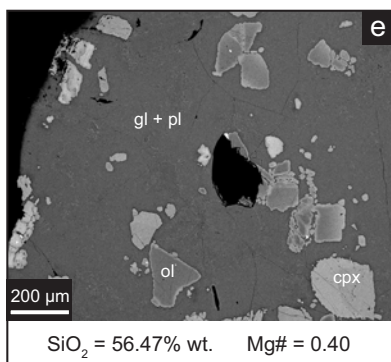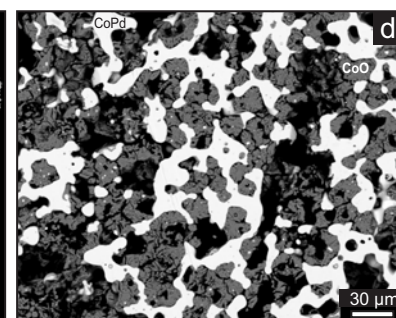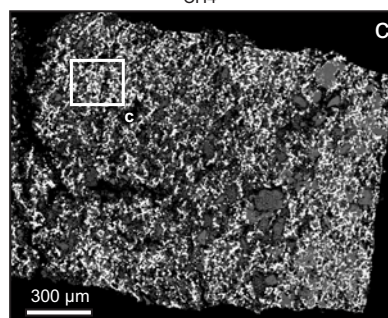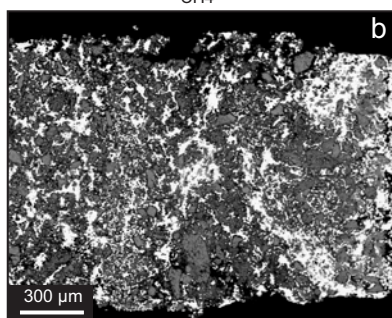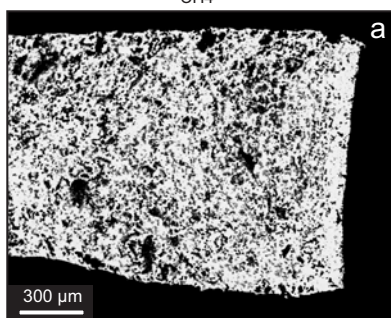
M22_fO$_2$_2

M22_fO$_2$_1

M22_fO$_2$_4

Close-up of M22_fO$_2$_4
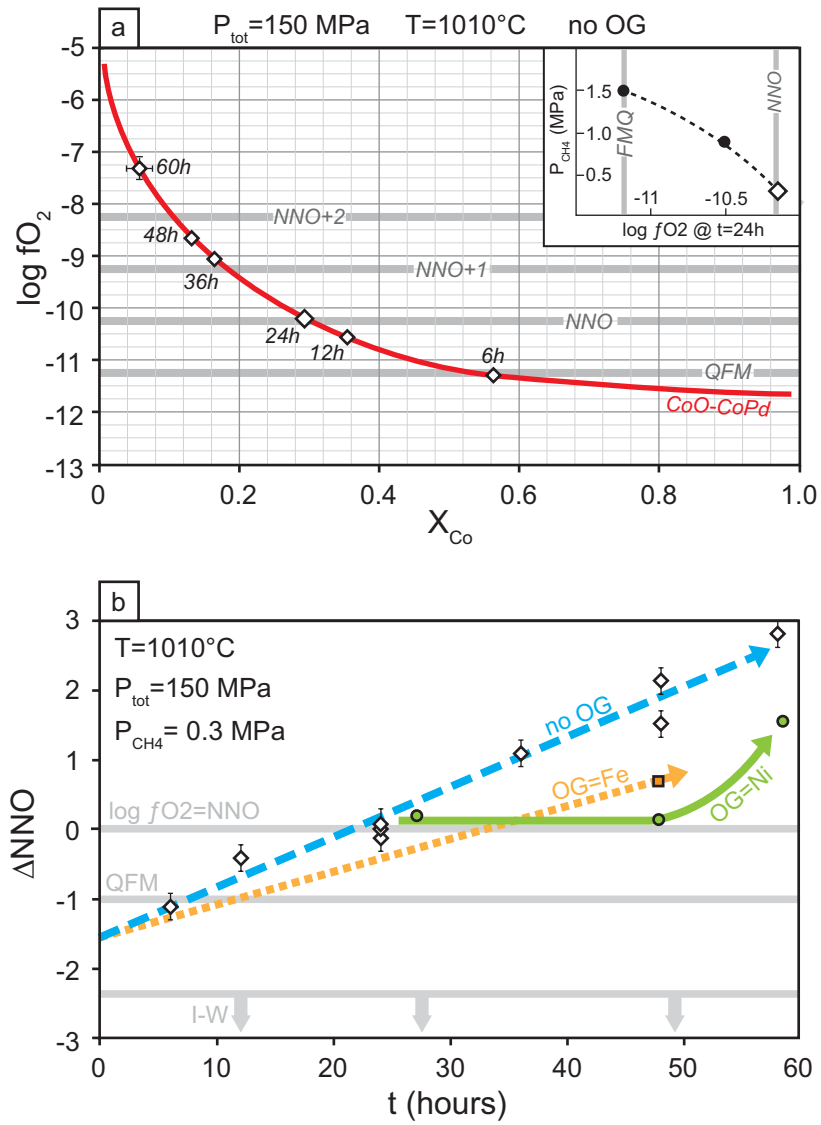
Figure 3
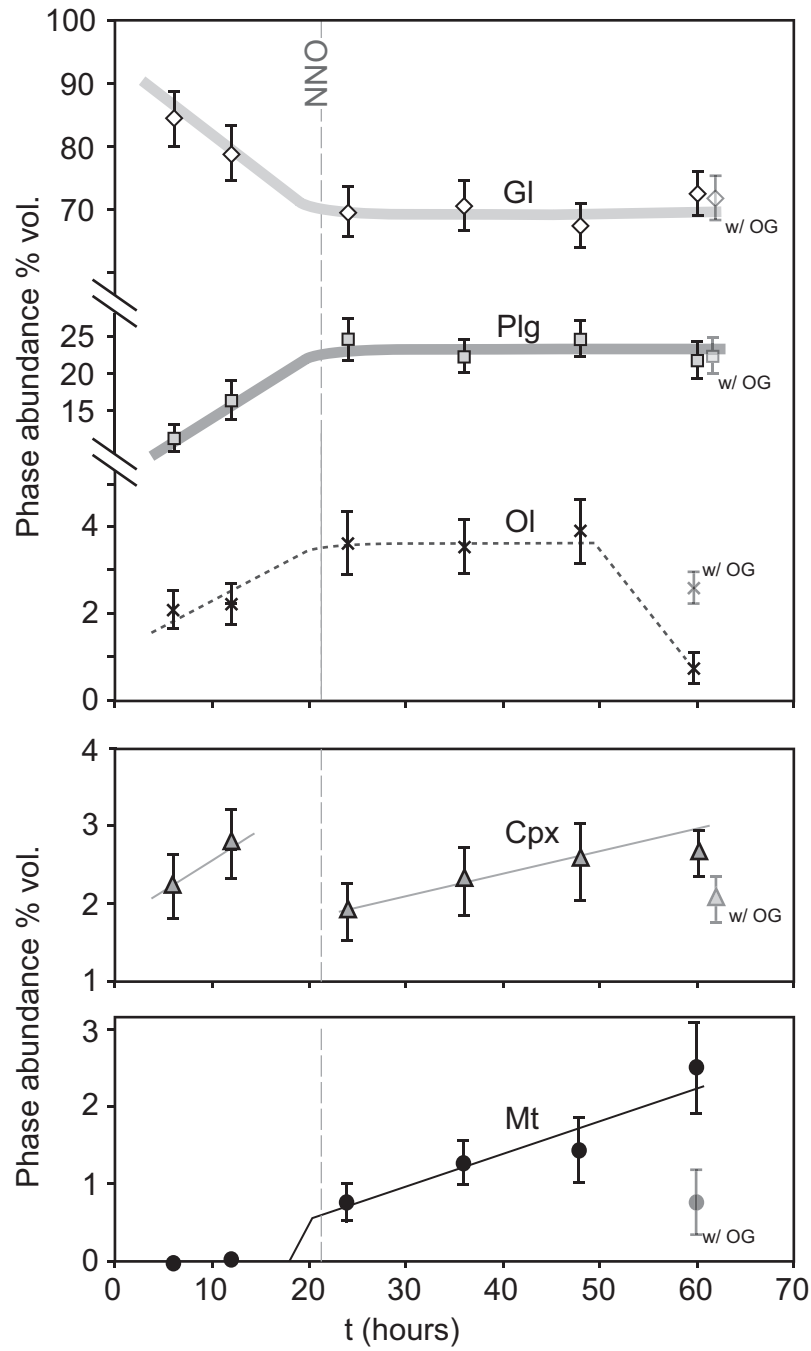
Figure 4
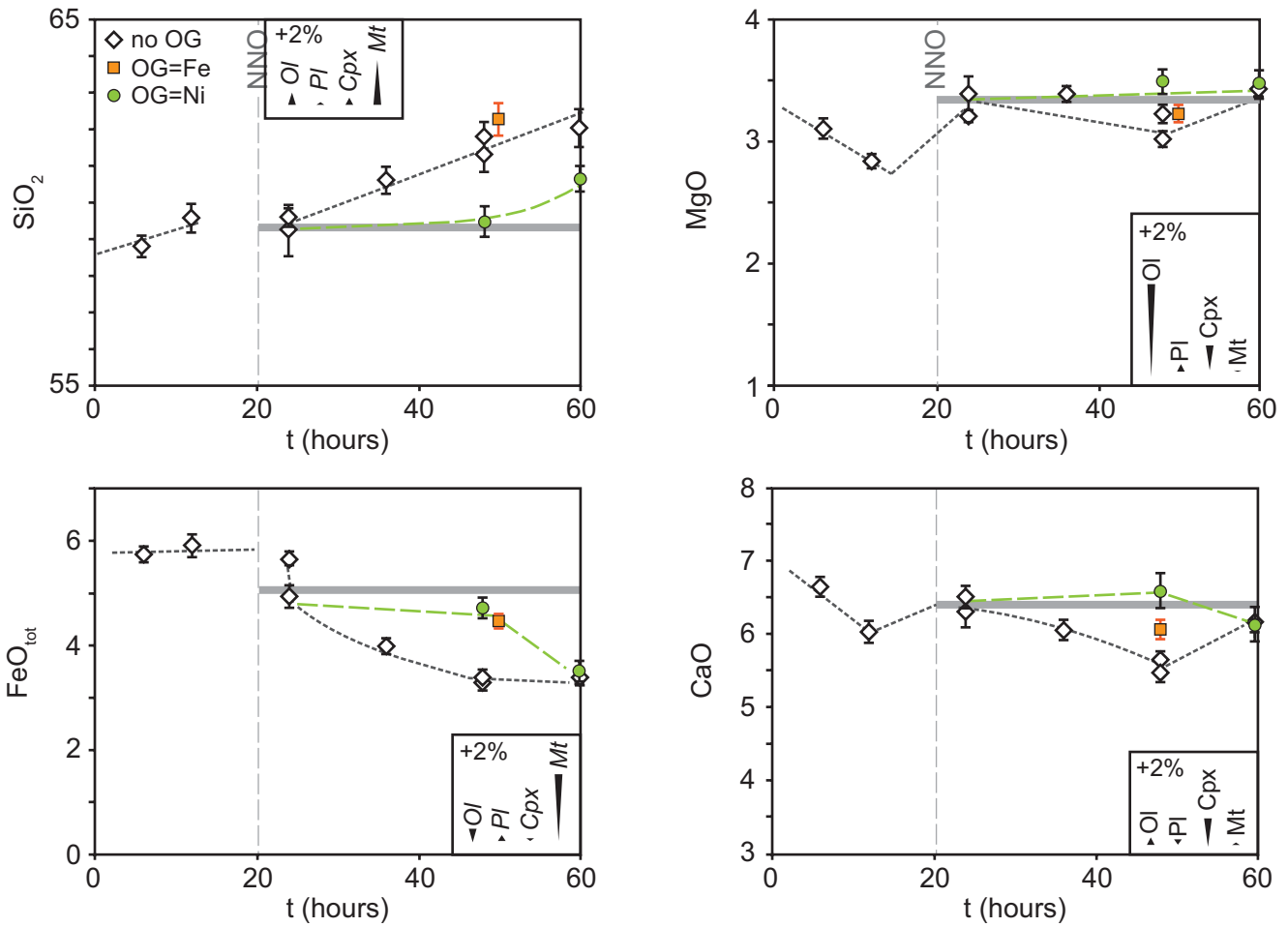
Figure 5

Table 1: Abridged list of hydrous experiments involving mafic magmas at high temperatures (i.e. having at least some runs with T≥950°C) carried out in cold-seal pressure vessels, and the techniques employed to control and monitor oxygen fugacity.

Study	Starting composition	setup	T (°C)[a]	P (MPa)[b]	t (h)[c]	fO2 control [d]	fO2 sensing [e]
Gaetani et al., 1994	Basaltic-andesite	CSPV	1005-1100	200	3-24	GP(Ar-CH$_4$), SB	-
Parman et al., 1997	Komatiite	CSPV	1026-1257	100-200	5-41	GP(Ar-CH$_4$), SB	-
Grove et al., 1997	Andesite	CSPV	865-1050	100-200	18-66	I, SB	-
Metrich and Rutherford, 1998	Basaltic-hawaiite	CSPV	1009-1135	27-80	8-38	GP(Ar-CH$_4$), SB	-
Dann et al., 2001	Fe-basalt	CSPV	960-1105	100-200	9-49	GP(Ar-CH$_4$), SB	-
Hammer et al., 2002	Andesite	CSPV	850-1050	50-225	22-96	GP(Ar-CH$_4$), SB	-
Szramek et al., 2006	Basaltic-andesite	CSPV	940-1075	50-200	8-30	GP(Ar-CH$_4$), SB	-
Barr et al., 2009	Komatiite	CSPV	1125-1275	180-210	3-7	GP(Ar-CH$_4$), SB	-
This study	Basaltic-andesite	CSPV	1010	150	6-60	GP(Ar-CH$_4$), SB	Co-Pd MS

a. Range of experimental temperatures investigated
b. Range of experimental pressures
c. Range of experimental durations
d. Method(s) utilized to impose oxygen fugacity
e. Method(s) utilized to measure oxygen fugacity

Abbreviations:
CSPV: Cold-seal pressure vessel
GP: Gas pressure control of fO2 by varying gas proportions
MS: Double capsule metal-metal oxide sensor technique (Taylor et al., 1992)
I: fO_2 intrinsically controlled by vessel alloy
SB: Solid buffer technique (see Eugster, 1957; Huebner, 1971)

Table 2: List of experiments with measured $f\mathrm{O}_2$ and phase abundances. All experiments were run at T=1010°C and P_{total}=150 MPa.

Experiment	t (h)	P_{CH4} (MPa)	OG[a]	X_{Co} (WDS)[b]	X_{Co} (EDS)[c]	log fO2[d]	ΔNNO[e]	ϕ_{Ol}[f]	ϕ_{Cpx}	ϕ_{Pl}	ϕ_{Mt}	ϕ_{Gl}
MAS_fO2_1	24	0.3	-	0.304(2)	0.293(6)	-10.28	-0.10					
MAS_fO2_1b	24	0.3	-		0.285(7)	-10.15	+0.03	0.036	0.019	0.245	0.008	0.692
MAS_fO2_2	24	1.5	-	0.517(6)	0.514(7)	-11.18	-1.00					
MAS_fO2_3	24	0.9	-	0.324(13)	0.338(10)	-10.48	-0.31					
MAS_fO2_4	48	0.3	-		0.132(7)	-8.66	+1.51	0.039	0.026	0.246	0.014	0.675
MAS_fO2_5	12	0.3	-		0.354(9)	-10.57	-0.39	0.022	0.028	0.163	0	0.786
MAS_fO2_6	36	0.3	-		0.164(12)	-9.06	+1.11	0.036	0.023	0.224	0.012	0.704
MAS_fO2_7	6	0.3	-		0.563(9)	-11.29	-1.11	0.021	0.022	0.112	0	0.845
MAS_fO2_8	24×2[†]	0.3×2[†]	-		0.902(7)	-8.02	+2.16					
MAS_fO2_9	24×3[*]	0.3×3[*]	-		0.514(7)	-11.18	-1.00					
MAS_fO2_10	48	0.3	Fe		0.208(17)	-9.52	+0.66					
MAS_fO2_13	48	0.3	Ni		0.268(4)	-10.03	+0.15					
MAS_fO2_15	60	0.3	Ni		0.130(7)	-8.64	+1.54	0.026	0.021	0.221	0.072	0.725
MAS_fO2_16	60	0.3	-		0.061(5)	-7.44	+2.74	0.007	0.026	0.211	0.025	0.730
MAS_fO2_17	48[§]	0.3, 5[§]	-		0.202(3)	-9.46	+0.72					
MAS_fO2_18	48[¥]	0.3[¥]	-		0.145(2)	-8.83	+1.34					

a. Presence and type of oxygen getter

b. Composition of CoPd alloy analyzed using EMPA (1 standard deviation in parentheses, numbers correspond to last digits)

c. Composition of CoPd alloy analyzed using SEM (1 standard deviation in parentheses, numbers correspond to last digits)

d. Log of oxygen fugacity calculated using the CoPd composition (see text).

e. Departure of log fO2 from the nickel-nickel-oxide buffer reaction

f. ϕ= phase abundance as fraction of total, with Ol=olivine, Cpx=clinopyroxene, Pl=plagioclase, Mt=magnetite, Gl=glass

[†] Experiment started with 0.3 MPa CH_4 replenished without quenching at t=24h

[*] Experiment that has been quenched and for which the initial CH_4 was replenished

[§] Experiment started with 0.3 MPa CH_4, and replenished with 5 MPa CH_4 with no quenching step at t=24h

[¥] Experiment similar to MAS_fO2_4 but with extra H_2O added to the sensor capsule

Table 3: Major element chemistry of experimental glasses.

Experiment	t (h)	SiO_2	TiO_2	Al_2O_3	FeO_{tot}	MnO	MgO	CaO	Na_2O	K_2O	P_2O_5	Totals
Variable: P_{CH4}												
MAS_fO2_1	24	56.86(0.84)	0.83(0.04)	18.21(0.21)	5.56(0.06)	0.10(0.01)	3.04(0.04)	6.43(0.10)	4.06(0.09)	1.49(0.03)	0.24(0.02)	96.82
MAS_fO2_1b	24	57.23(0.16)	0.86(0.05)	17.78(0.21)	4.78(0.19)	0.11(0.02)	3.30(0.14)	6.16(0.19)	3.99(0.08)	1.49(0.04)	0.30(0.06)	95.99
MAS_fO2_2	24	56.47(0.34)	0.80(0.01)	18.21(0.11)	5.35(0.11)	0.10(0.02)	3.56(0.08)	7.12(0.06)	4.07(0.07)	1.33(0.03)	0.25(0.01)	97.32
MAS_fO2_3	24	57.36(0.14)	0.88(0.02)	17.64(0.22)	5.65(0.11)	0.11(0.01)	3.24(0.15)	6.03(0.25)	4.08(0.09)	1.44(0.05)	0.27(0.03)	96.70
Variable: time												
MAS_fO2_4	48	59.32(0.27)	0.85(0.04)	18.14(0.17)	3.37(0.04)	0.09(0.01)	2.91(0.05)	5.24(0.05)	4.58(0.11)	1.73(0.04)	0.32(0.03)	96.54
MAS_fO2_5	12	57.63(0.37)	0.91(0.02)	17.71(0.08)	5.63(0.14)	0.11(0.01)	2.75(0.04)	5.85(0.09)	4.24(0.09)	1.59(0.06)	0.29(0.03)	96.72
MAS_fO2_6	36	58.19(0.34)	0.89(0.03)	17.76(0.10)	3.89(0.12)	0.09(0.01)	3.25(0.04)	5.84(0.08)	4.25(0.08)	1.55(0.02)	0.28(0.04)	96.01
MAS_fO2_7	6	57.17(0.23)	0.88(0.03)	18.03(0.11)	5.60(0.09)	0.11(0.02)	3.02(0.06)	6.47(0.09)	4.11(0.08)	1.54(0.05)	0.30(0.06)	97.23
MAS_fO2_8	48	58.77(0.42)	0.84(0.05)	17.80(0.12)	3.34(0.10)	0.09(0.01)	3.11(0.07)	5.40(0.10)	4.22(0.10)	1.58(0.02)	0.29(0.02)	95.46
MAS_fO2_16	60	60.61(0.24)	0.75(0.04)	18.01(0.13)	3.34(0.04)	0.08(0.01)	3.31(0.04)	5.98(0.05)	4.01(0.38)	1.39(0.02)	0.25(0.03)	97.80
Variable: OG												
MAS_fO2_13	48	57.73(0.29)	0.77(0.04)	18.14(0.16)	4.32(0.16)	0.09(0.01)	3.43(0.06)	6.47(0.16)	4.10(0.08)	1.39(0.08)	0.24(0.02)	96.69
MAS_fO2_15	60	58.30(0.37)	0.79(0.04)	16.32(0.15)	3.32(0.13)	0.08(0.01)	3.34(0.19)	5.80(0.21)	4.07(0.11)	1.39(0.09)	0.25(0.03)	95.76